Journal of Power Sources 270 (2014) 257–261

Contents lists available at ScienceDirect

Journal of Power Sources

journal homepage: www.elsevier.com/locate/jpowsour

Short communication

Copper@palladium–copper core–shell nanospheres as a highly effective electrocatalyst for ethanol electro-oxidation in alkaline media

Jindi Cai, Yanzhen Zeng, Yonglang Guo*

College of Chemistry, Fuzhou University, Fuzhou 350116, PR China

HIGHLIGHTS

- The Cu@PdCu/C catalyst is synthesized via the galvanic replacement method.
- The nanoparticles present core–shell structure with the shell thickness of about 0.5 nm.
- Ethanol oxidation peak current on Cu@PdCu/C is 2.78 times higher than that on Pd/C.
- Durability and anti-poisoning ability of Cu@PdCu/C toward ethanol oxidation are greatly promoted.
- The promoted effect is due to the synergistic effect between Pd and Cu.

GRAPHICAL ABSTRACT

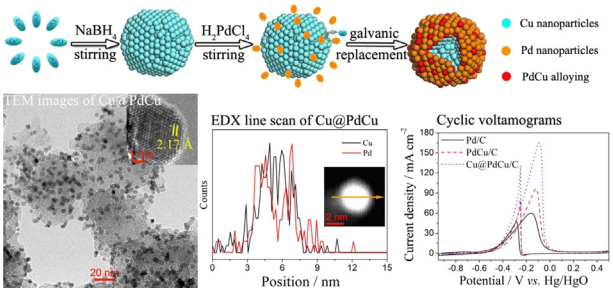

ARTICLE INFO

Article history:
Received 18 May 2014
Received in revised form
18 July 2014
Accepted 21 July 2014
Available online 26 July 2014

Keywords:
Alkaline media
Core–shell structure
Ethanol oxidation
Palladium-based catalyst
Palladium–Copper

ABSTRACT

A novel Cu@PdCu/C catalyst with the core–shell structure is prepared by the galvanic replacement between Pd^{2+} ions and Cu particles. It is characterized by X-ray diffraction (XRD), X-ray photoelectron spectroscopy (XPS), transmission electron microscopy (TEM), energy-dispersive X-ray spectra (EDX) and electrochemical measurements. The Cu@PdCu nanoparticles are composed of the Cu core and PdCu alloying shell with a thickness of ca. 0.5 nm. The peak current density of ethanol oxidation on Cu@PdCu/C is 166.0 mA cm^{-2}, which is 2.78 times higher than that on Pd/C catalyst (59.8 mA cm^{-2}). Durability and poisoning tolerance of this catalyst are also greatly improved.

1. Introduction

Recently, direct ethanol fuel cell (DEFC) has received a great number of attentions. This is because ethanol has non-toxicity, low permeability and high theoretical mass energy density (8.01 kWh kg^{-1}) as compared with methanol. And ethanol can be easily produced in great quantities from the fermentation of biomass [1–3]. A lot of researches showed that the electro-oxidation reaction of ethanol presented high activity in alkaline medium [4,5]. Pd is considered to be a promising alternative to Pt on alcohol electro-oxidation in alkaline medium [6]. It is well known that the alloying of Pd with other metals or its combination with metal oxides can remarkably enhance both their catalytic activity and stability for alcohol oxidation in alkaline solution [6,7].

* Corresponding author. Tel./fax: +86 591 8807 3608.
E-mail address: yguo@fzu.edu.cn (Y. Guo).

http://dx.doi.org/10.1016/j.jpowsour.2014.07.131
0378-7753/

Apart from the effects by elements, the sizes and morphologies of electrocatalysts also have a crucial influence on the catalytic activity [8,9].

The tailored design and synthesis of core–shell nanoparticle catalyst is an effective method to enhance the catalytic activity [10–14]. The design with noble metal as thin shell on proper non-noble metal core not only reduces the usage of noble metal, but also significantly enhances the catalytic performance due to the so-called strain and ligand effect between the core substrate and the noble metal shell [15–17]. The polyvinylpyrrolidone (PVP) is used to synthesize core–shell catalysts in numerous researches. However, the capping agents are difficult to be removed completely and prone to block the catalytic active sites and enlarge the nanoparticle size [18]. A galvanic displacement method is developed to prepare core–shell catalysts without the use of capping agents. The catalysts with ultralow noble metal loadings can be easily synthesized by this method.

The cheep cupreous material is a promising assistant for Pt-based catalysts, but only a handful of studies focus on alcohol oxidation using Pd–Cu catalysts with well-defined morphologies in alkaline media [19–21]. In this study, the Cu@PdCu core–shell nanoparticles were prepared by the galvanic replacement between Pd^{2+} ions and Cu particles. The Cu@PdCu/C catalyst has much higher catalytic activity and stability toward ethanol oxidation as compared with state-of-the-art Pd/C and PdCu/C catalysts.

2. Experimental

2.1. Synthesis of Cu@PdCu/C catalyst

The active carbon black (Vulcan XC-72R) used in this work was purchased from Cabot Corp. (USA). The processes of purification and acid-functionalization are described in detail elsewhere [22]. Prior to the synthesis, all solvents used were de-aerated with N_2 for 30 min. 17.8 mg of Vulcan XC-72R carbon and 0.3 g sodium citrate were dissolved in 50 ml of ethylene glycol (EG) under ultrasonic stirring. 4 ml of $CuSO_4$ (18.9 mM) solution was added into the suspension with constant stirring for 30 min. Then 25 ml of freshly prepared $NaBH_4$ (20 mM) solution was added dropwise under vigorous stirring at room temperature. The mixture was stirred for one night to decompose any remaining $NaBH_4$. After that, 1 ml of H_2PdCl_4 (37.8 mM) solution was added into the mixture. The Cu@PdCu/C catalyst was synthesized by the galvanic displacement reaction of $PdCl_4^{2-}$ to Pd via oxidizing Cu. The reaction in the mixture was conducted for one day under stirring. The entire reaction process was performed under N_2 atmosphere to prevent oxidation of Cu nanoparticles. Finally, the black product was filtered, washed and dried in a vacuum oven at 80 °C for 8 h. For comparison, PdCu/C and Pd/C were synthesized directly by co-reduction of the metal precursor using the dropwise addition of $NaBH_4$ under nitrogen atmosphere at room temperature.

2.2. Physical and electrochemical characterization

Characterization of as-prepared catalysts was tested under similar conditions as reported in Ref. [22]. Atomic adsorption spectroscopy (AAS, TAS-686G) was used to analyze the compositions of as-prepared catalysts. The XRD patterns were obtained from an X-ray powder diffractometer (Philip X' Pert Pro MPP) using a CuKα radiation ($\lambda = 1.5418$ Å) at the scan rate of 2° min^{-1} with a step of 0.02°. The chemical valence states of the catalysts were analyzed by the X-ray photoelectron spectroscopy (XPS, VG ESCALAB 250) using an Al Kα X-ray source of 1486.6 eV. The morphology and size distribution of the catalysts were examined using a transmission electron microscope (TEM, JEOL JEM-2010). Energy-dispersive X-ray (EDX) analysis was carried out by a microanalyser. And an FEI Tecnai G2 F20 S-Twin TEM equipped with an EDX detector was employed for the high-angle annular dark-field scanning TEM (HAADF-STEM) images and EDX line analysis.

Electrochemical measurements were carried out by a CHI 660C electrochemical working station (CH Instrument Inc.) in a typical three-electrode electrolytic cell. Glassy carbon electrode (GCE, 0.1256 cm^2) was used as the working electrode to support the catalysts. A piece of Pt foil and the mercuric oxide electrode (Hg/HgO/1 M KOH, 0.098 V *vs.* SHE) were used as the counter and reference electrodes, respectively. For the working electrode preparation, 5.0 mg as-prepared catalyst was dispersed in 1 ml solution of 985 μl isopropyl alcohol and 15 μl Nafion solution (15 wt %, DuPont) under ultrasonic stirring for 30 min. A 4 μl aliquot of the slurry was transferred onto the pre-polished GCE by using a micropipette and dried under an infrared lamp. Before measurements, the electrolyte was first de-aerated with high purity N_2. All electrochemical measurements were performed at 30 ± 1 °C, as reported in Ref. [22].

3. Results and discussion

The Pd loadings and chemical compositions of the as-prepared Pd/C, PdCu/C and Cu@PdCu/C catalysts were determined using AAS analysis, respectively, as shown in Table 1. It is found that the galvanic replacement of Cu nanoparticle core with Pd^{2+} was not completed for the Cu@PdCu/C catalyst because its theoretical content of Pd is 20 wt% and atomic ratio of Pd:Cu is 1:1. The XRD patterns of Pd/C, PdCu/C and Cu@PdCu/C catalysts are shown in Fig. 1A. At about 25°, all diffractograms show a broad peak which refers to graphite (002) facet of carbon black. In the XRD pattern of Pd/C, the four main diffraction peaks located at about 39.8°, 46.3°, 67.6° and 81.2° are ascribed to the (111), (200), (220) and (311) reflections of face centered cubic (*fcc*) Pd crystal (JCPDS Card No. 05-0681), respectively. For PdCu/C and Cu@PdCu/C catalysts, these four main diffraction peaks shift in positive position, which suggests the alloying between Pd and Cu. Fig. 1B shows the survey XPS spectra of these three catalysts. All catalysts have Pd 3d spectra, as shown in Fig. 1C. The binding energy of Pd signals have shifted negatively on PdCu/C and Cu@PdCu/C catalysts as compared with that on Pd/C catalyst, indicating the electronic interaction between Pd and Cu atoms. Pd 3d spectra can be deconvoluted into two pairs of peaks, which are ascribed to metallic Pd(0) and Pd(II) species. Moreover, the Cu 2p spectra can be found in the XPS spectra of PdCu/C and Cu@PdCu/C catalysts (shown in Fig. 1D). In the Cu 2p region, the deconvoluted peaks are assigned to metallic Cu(0) and Cu(II) species as well as the satellite peak of CuO (at ~943.0 eV) [20]. The Cu 2p signal of Cu@PdCu/C is intense, which suggests that part of Cu exists on the catalyst surface [23]. In addition, the compositions of these three catalysts analyzed by XPS are also shown in Table 1. It is found that the content of Cu in Cu@PdCu/C obtained from XPS is obviously lower than that in the noumenon of Cu@PdCu/C analyzed by AAS, demonstrating that part of Cu atoms at the surface of the Cu core is displaced by Pd^{2+} to form the

Table 1
The compositions obtained from AAS and XPS as well as particle sizes from TEM images for as-prepared catalysts.

Samples	Contents of Pd (wt%)	Atomic ratios from AAS (Pd:Cu)	Atomic ratios from XPS (Pd:Cu)	Particle sizes (nm)
Pd/C	19.68	/	/	3.0
PdCu/C	20.16	1:0.84	1:0.78	2.7
Cu@PdCu/C	16.92	1:1.46	1:0.46	3.9

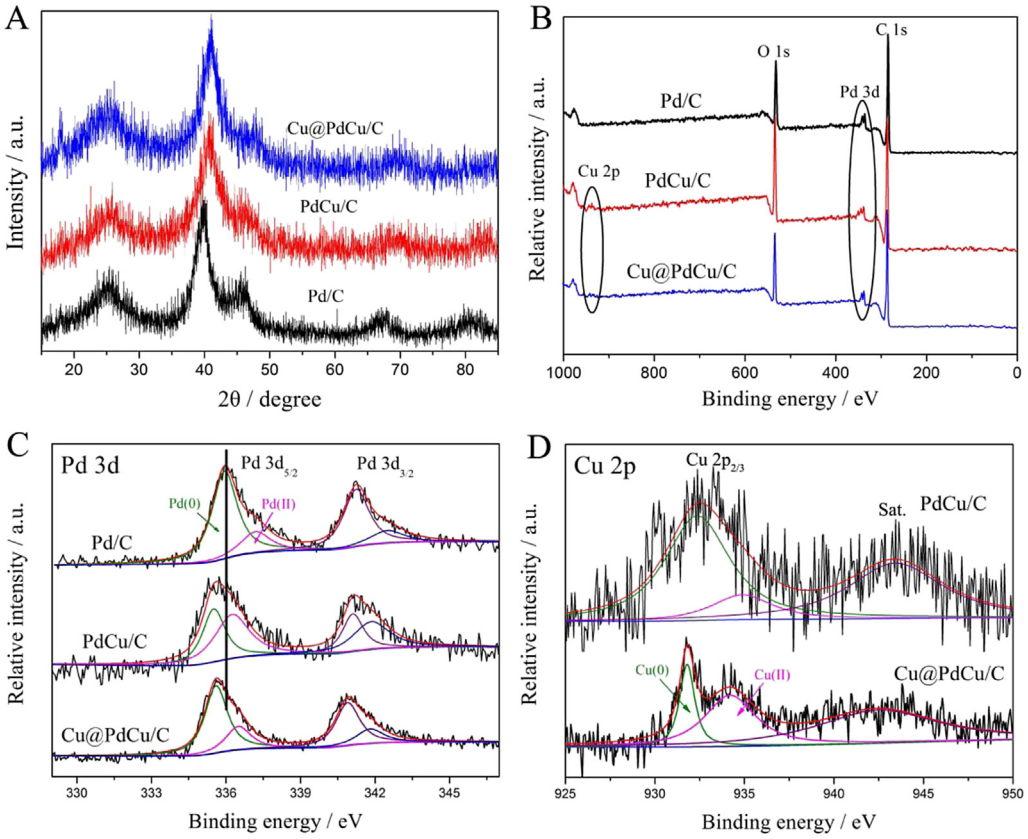

Fig. 1. (A) XRD patterns and (B) XPS survey spectra of the Pd/C, PdCu/C and Cu@PdCu/C catalysts; High-resolution XPS spectra of (C) Pd 3d and (D) Cu 2p regions.

Cu@PdCu nanoparticles which have the core–shell structure with Cu core and PdCu alloying shell.

The TEM images of Pd/C, PdCu/C and Cu@PdCu/C catalysts are shown in Fig. 2A, B and C, respectively. The insets in Fig. 2A, B and C present the high-resolution TEM (HRTEM) images of these three catalysts. Most of metal nanoparticles are uniformly dispersed on carbon surface. The lattice distance with 2.26 Å is indexed to the Pd (111) in Pd/C, simultaneously 2.18 and 2.17 Å are attributed to PdCu (111) planes in PdCu/C and Cu@PdCu/C catalysts, respectively. The particle size distributions of the nanoparticles in these three catalysts were determined by the statistic analysis of more than 500 particles in arbitrarily selected area of the corresponding TEM images and these results are shown in Table 1. EDX analysis of Cu@PdCu/C catalyst is shown in Fig. 2D. The Cu@PdCu/C catalyst is composed of C, Pd and Cu (The Mo signal comes from the sample holder). From the HAADF-STEM image of Cu@PdCu/C in Fig. 2E, the corresponding line-profile analysis was performed and presented in Fig. 2F. The EDX line scan along with the origin arrow line in Fig. 2E was conducted to analyze the structure of the Cu@PdCu nanoparticle. In the scanning across the particle, the Pd and Cu contents rise quickly on both sides of the particle and the Cu content reaches the highest while the Pd content drops very low in the center section. This phenomenon is characteristic of the core–shell structure for Cu@PdCu nanoparticle. Moreover, a PdCu alloying shell with a 0.5 nm thickness is obtained from the HAASF-STEM image and its corresponding line-profile analysis.

The electrochemical performances of as-prepared catalysts are shown in Fig. 3. The cyclic voltamograms (CVs) in Fig. 3A were obtained in 1 M KOH solution. The catalysts exhibit the hydrogen adsorption/desorption peaks in the potential region of −0.95 ~ −0.65 V. It can be observed that the peak currents of hydrogen adsorption/desorption greatly decrease on PdCu/C and Cu@PdCu/C catalysts. Besides, an obvious oxidation peak appears at about −0.04 V on PdCu/C and Cu@PdCu/C catalysts and is attributed to the formation of Cu oxides on the catalyst surface [21,24]. Moreover, the reduction peak at about −0.29 V becomes higher and shifts a little in negative direction on PdCu/C and Cu@PdCu/C compared with Pd/C, which is ascribed to the simultaneous reduction of PdO and Cu oxides [24]. Ethanol electro-oxidation on the as-prepared catalysts is shown in Fig. 3B. The oxidation peak currents of ethanol on Cu@PdCu/C, PdCu/C and Pd/C catalysts are 166.0, 96.9 and 59.8 mA cm^{-2}, respectively. The Cu@PdCu/C catalyst presents the best electrocatalytic activity for ethanol oxidation among these catalysts, which is mainly due to the synergistic effect between Pd and Cu (such as geometric effect, electronic effect and bifunctional mechanism, etc.) in the Cu@PdCu/C catalyst with special core–shell structure. Besides, the ratio of forward to backward peak current (I_f/I_b) on Cu@PdCu/C is the highest (1.36), indicating it has the highest tolerance toward intermediate species among these catalysts [23]. The electrocatalytic stability of the as-prepared catalysts for ethanol oxidation was studied by the chronoamperometry in 1 M KOH +1 M C_2H_5OH solution at −0.3 V, as shown in Fig. 3C. After an initial quick drop in performance, the activity were stabilized at 10.8 mA cm^{-2} on Cu@PdCu/C, 3.5 mA cm^{-2} on PdCu/C and 1.2 mA cm^{-2} on Pd/C, respectively. Cu@PdCu/C catalyst shows the highest current in the whole process among the three catalysts, indicating its best catalytic durability towards ethanol oxidation. As observed in Fig. 3D, the ethanol oxidation current on Cu@PdCu/C catalyst remains 74.1% after 1000 CV cycles, which is the highest among these catalysts. This further demonstrates that Cu@PdCu/C catalyst has the best durability and stability for ethanol oxidation. The linear current sweep

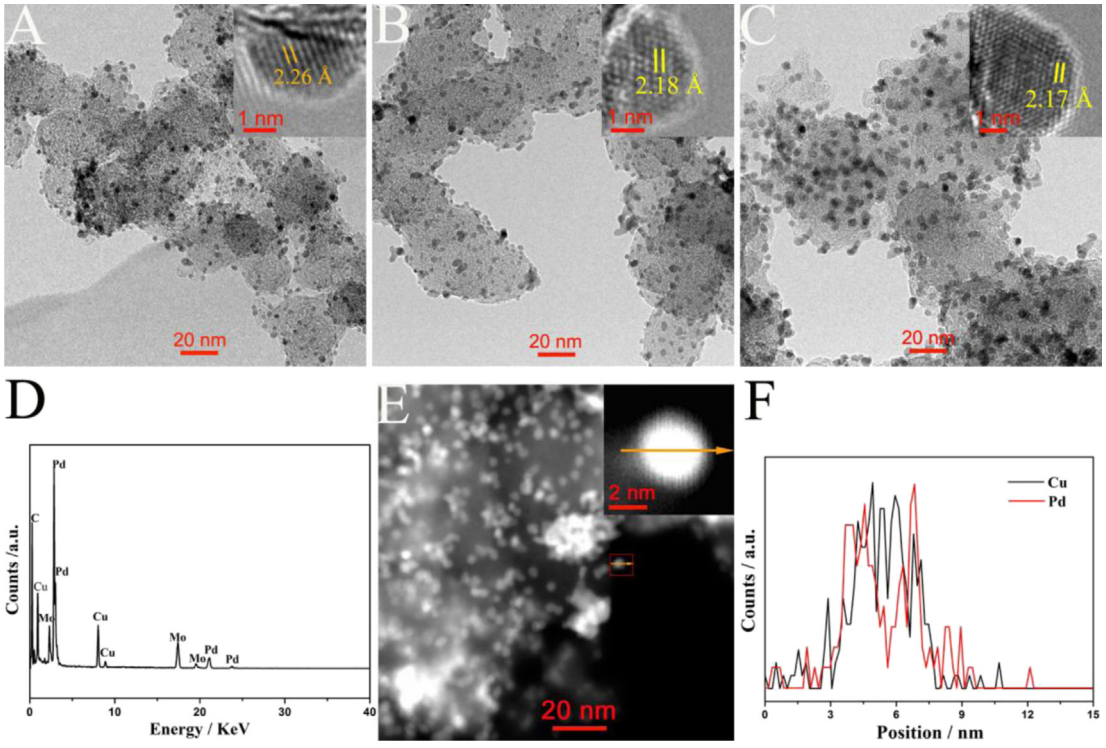

Fig. 2. The low-magnification TEM images of (A) Pd/C, (B) PdCu/C and (C) Cu@PdCu/C catalysts. The insets are the corresponding high-resolution TEM images; (D) the EDX spectrum of Cu@PdCu/C; (E) HAADF-STEM images of Cu@PdCu/C. The inset is the high-magnification HAADF-STEM image; (F) its line profile analysis along with the line in panel E.

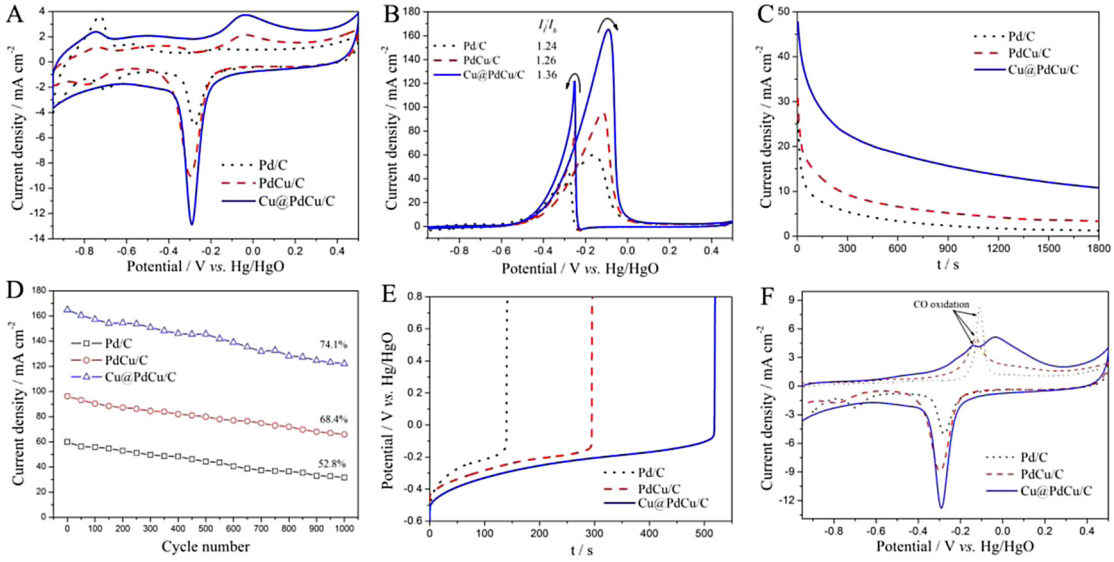

Fig. 3. Cyclic voltammograms of the as-prepared catalysts in (A) 1 M KOH and (B) 1 M KOH + 0.5 M C_2H_5OH solutions. Scan rate: 50 mV s^{-1}. (C) Current–time curves at −0.3 V and (D) long-term stabilities and (E) linear current sweep at 0.16 mA cm^{-2} s^{-1} for the as-prepared catalysts in 1 M KOH + 1 M C_2H_5OH solution; (F) CO stripping curves of the as-prepared catalysts in 1 M KOH. Scan rate: 50 mV s^{-1}.

experiment was acquired at the scan rate of 0.16 mA cm^{-2} s^{-1} in 1 M KOH +1 M C_2H_5OH solution, as shown in Fig. 3E. It is clearly shown that the Cu@PdCu/C catalyst has the lowest polarization potential platform and the longest polarization time of 520 s at the point of steep hop in potential, suggesting that Cu@PdCu/C catalyst exhibits best poisoning tolerance towards poisonous intermediate species [22]. Fig. 3F depicts CO stripping curves of these three catalysts. The peak potentials for CO oxidation on Cu@PdCu/C, PdCu/C and Pd/C catalysts are −0.140, −0.126 and −0.108 V, respectively. Besides, Cu@PdCu/C has the lower onset potential and smaller peak for CO oxidation as compared with PdCu/C and Pd/C catalysts, indicating its good tolerance towards CO poisoning [4].

4. Conclusions

In summary, a novel Cu@PdCu/C catalyst was prepared by the galvanic replacement method. The Cu@PdCu particles consisted of the Cu core and a PdCu alloying shell of about 0.5 nm thickness. The

Cu@PdCu/C catalyst with core–shell structure increases Pd utilization, enlarges the specific surface area and provides more Pd active sites for ethanol oxidation. Moreover, the synergistic effect between Pd and Cu improves the electrochemical performance of Cu@PdCu/C catalyst. The peak current of ethanol oxidation on Cu@PdCu/C catalyst is very high and reaches 166.0 mA cm^{-2}. Beside, its durability and anti-poisoning ability are notably promoted. Thus, the superior performance of Cu@PdCu/C makes it a feasible anodic electrocatalyst in alkaline direct ethanol fuel cells.

Acknowledgments

Financial support from the National Natural Science Foundation of China (No. 51072037) and Natural Science Foundation of Fujian Province (No. 2013J01039) in this work is gratefully acknowledged.

References

[1] E. Antolini, J. Power Sources 170 (2007) 1.
[2] S. Song, P. Tsiakaras, Appl. Catal. B 63 (2006) 187.
[3] L. Jiang, G. Sun, S. Wang, G. Wang, Q. Xin, Z. Zhou, B. Zhou, Electrochem. Commun. 7 (2005) 663.
[4] K. Wu, X. Mao, Y. Liang, Y. Chen, Y. Tang, Y. Zhou, J. Lin, C. Ma, T. Lu, J. Power Sources 219 (2012) 258.
[5] S.C.S. Lai, M.T.M. Koper, Phys. Chem. Chem. Phys. 11 (2009) 10446.
[6] E. Antolini, Energy Environ. Sci. 2 (2009) 915.
[7] E. Antolini, E.R. Gonzalez, J. Power Sources 195 (2010) 3431.
[8] N. Tian, Z. Zhou, S. Sun, Y. Ding, Z. Wang, Science 316 (2007) 732.
[9] X. Huang, S. Tang, X. Mu, Y. Dai, G. Chen, Z. Zhou, F. Ruan, Z. Yang, N. Zheng, Nat. Nanotechnol. 6 (2011) 28.
[10] R. Zhao, M. Gong, H. Zhu, Y. Chen, Y. Tang, T. Lu, Nanoscale 6 (2014) 9273.
[11] W. Zhou, J.Y. Lee, Electrochem. Commun. 9 (2007) 1725.
[12] M. Zhang, Z. Yan, J. Xie, Electrochim. Acta 77 (2012) 237.
[13] Y. Zhao, X. Yang, J. Tian, F. Wang, L. Zhan, Int. J. Hydrogen Energy 35 (2010) 3249.
[14] J. Chen, Y. Li, Z. Gao, G. Wang, J. Tian, C. Jiang, S. Zhu, R. Wang, Electrochem. Commun. 37 (2013) 24.
[15] K. Tedsree, T. Li, S. Jones, C.W.A. Chan, K.M.K. Yu, P.A.J. Bagot, E.A. Marquis, G.D.W. Smith, S.C.E. Tsang, Nat. Nanotechnol. 6 (2011) 302.
[16] P. Strasser, S. Koh, T. Anniyev, J. Greeley, K. More, C.F. Yu, Z.C. Liu, S. Kaya, D. Nordlund, H. Ogasawara, M.F. Toney, A. Nilsson, Nat. Chem. 2 (2010) 454.
[17] H. Kobayashi, M. Yamauchi, H. Kitagawa, Y. Kubota, K. Kato, M. Takata, J. Am. Chem. Soc. 130 (2008) 1818.
[18] N. Muthuswamy, J.L.G. de la Fuente, D.T. Tran, J. Walmsley, M. Tsypkin, S. Raaen, S. Sunde, M. Rønning, D. Chen, Int. J. Hydrogen Energy 38 (2013) 16631.
[19] M. Gong, G. Fu, Y. Chen, Y. Tang, T. Lu, ACS Appl. Mater. Interfaces 6 (2014) 7301.
[20] M. Ammam, E.B. Easton, J. Power Sources 222 (2013) 79.
[21] W. Kang, Y. Wei, C. Liu, K. Wang, Electrochem. Commun. 13 (2011) 162.
[22] J. Cai, Y. Huang, Y. Guo, Electrochim. Acta 99 (2013) 22.
[23] Y. Huang, J. Cai, S. Zheng, Y. Guo, J. Power Sources 210 (2012) 81.
[24] Y. Huang, Y. Guo, Y. Wang, J. Power Sources 249 (2014) 9.